

# A mixed one-equation subgrid model for large-eddy simulation

Siniša Krajnović\*, Lars Davidson

*Department of Thermo and Fluid Dynamics, Chalmers University of Technology, SE-412 96 Göteborg, Sweden*

Received 10 July 2001; accepted 17 November 2001

## Abstract

A new mixed one-equation subgrid-scale (SGS) model for large-eddy simulation is presented. The scale-similarity part of the model is used for the description of the local energy transport (Domaradzki et al., 1993, 1994), i.e. the energy transport between scales very close to the cut-off. The eddy-viscosity part of the model represents the non-local transfer of energy, i.e. the transfer between all scales smaller than grid-filter size  $\Delta$  and larger than  $\Delta$ . A priori tests done by Bardina et al. (1980) have shown a high correlation between the scale-similarity model and the exact SGS stress,  $\tau_{ij}$ . The magnitude of the scale-similarity part in the mixed one-equation SGS model is either larger than or equal to that of the eddy-viscosity part. The modeled SGS stress is thus expected to correlate well with the exact stress,  $\tau_{ij}$ . In the proposed model, the SGS kinetic energy,  $k_{sgs}$ , is used to obtain the velocity scale for the eddy-viscosity part of the model. The modeled  $k_{sgs}$  equation is derived and contains some additional scale-similarity parts as compared with the  $k_{sgs}$  equation used in the models of Ghosal et al. (1995) or Davidson (1997). It has been shown that the model is Galilean invariant and realizable. Moreover, the approximately correct near-wall behavior of the model has been proven. The model was tested for both channel flow and the case of a surface-mounted cube (Martinuzzi and Tropea, 1993). It was found that the model gives accurate results in both cases. © 2001 Elsevier Science Inc. All rights reserved.

*Keywords:* Large-eddy simulation; Mixed dynamic subgrid-scale model; Subgrid-scale kinetic energy

## 1. Introduction

The energy transfer between large and small scales is mainly between the scales closest to the cut-off. The scale-similarity models (Bardina et al., 1980) are founded upon this argument. These models use the correlation between the smallest resolved scales and the largest unresolved scales in large-eddy simulation to model the main part of the subgrid-scale (SGS) energy. They are always used together with some dissipative model such as the Smagorinsky model under the name mixed models. In early simulations using mixed models (Bardina et al., 1980; Piomelli et al., 1988), the constant in the Smagorinsky model was prescribed a priori. Zang et al. (1993) used this model in the dynamic mode in the simulation of recirculating flows. The SGS model should be capable of covering a large part of the turbulent kinetic energy in an attempt to make LES a practical tool for complex flows at high Reynolds numbers. A large

part of the SGS energy is modeled with the scale-similarity part. Still, a significant amount of the SGS energy in a coarse LES remains to be represented by the Smagorinsky model, see Sarghini and Piomelli (1999). The Smagorinsky model assumes the isotropy of the small scales. Obviously this model is not suitable for modeling a significant part of the SGS energy resulting from the scales with evident anisotropic character. It does not contain any information on the SGS energy. The SGS velocity scale of the Smagorinsky model,  $|\mathcal{S}| = (2\bar{S}_{ij}\bar{S}_{ij})^{1/2}$ , is strongly affected by the mean flow. On the other hand, the smallest unresolved scales are assumed not to be correlated with the large scales (Bardina et al., 1980). Clearly, a more suitable model containing some information about the SGS energy is needed for modeling the smallest SGS scales.

In a coarse LES, a substantial fraction of the energy is in the SGS motion, indicating the need for constructing a more accurate model. This can be achieved by incorporating a history effect through the transport equation for the SGS kinetic energy. A model of this kind is the localized dynamic  $k_{sgs}$  equation model of Ghosal et al. (1995). However, the additional

\* Corresponding author.

E-mail address: sinisa@tfd.chalmers.se; www.tfd.chalmers.se/~lada/projects/sinisa/proright.html (S. Krajnović).

## Nomenclature

$C(x, y, z, t)$	space and time-dependent coefficient	$y^+$	$u_\tau y/\nu$
$C_{\text{hom}}(t)$	homogeneous coefficient	<i>Greeks</i>	
$C_\varepsilon$	dissipation coefficient	$\underline{\Delta}$	grid-filter size
$C_K$	convection term in $K$ equation	$\Delta$	test-filter size
$C_{k_{\text{sgs}}}$	convection term in $k_{\text{sgs}}$ equation	$\delta$	half channel height
$C_{\text{SS}}$	damping constant	$\varepsilon_K$	dissipation term in $K$ equation
$D_K$	diffusion term in $K$ equation	$\varepsilon_{k_{\text{sgs}}}$	dissipation term in $k_{\text{sgs}}$ equation
$D_{k_{\text{sgs}}}$	diffusion term in $k_{\text{sgs}}$ equation	$\nu_{\text{sgs}}$	subgrid-scale turbulent viscosity
$H$	cube height	$\nu$	laminar viscosity
$k_{\text{sgs}}$	subgrid-scale kinetic energy	$\Pi$	production term in $k_{\text{sgs}}$ equation (dissipation term in $\bar{k}$ equation)
$K$	subgrid-scale kinetic energy on the test level	$\Pi_{k_{\text{sgs}}}$	eddy-viscosity part of the SGS dissipation of the resolved kinetic energy
$k$	turbulent kinetic energy	$\Pi^{\text{SS}}$	scale-similarity part of the SGS dissipation of the resolved kinetic energy
$\bar{k}$	resolved kinetic energy	$\Pi_K$	production term in $K$ equation
$L_{ij}$	resolved Leonard stress	<i>Superscripts</i>	
$p$	pressure	EV	eddy-viscosity
$Re_\tau$	Reynolds number based on the friction velocity	M	modeled
$\bar{S}_{ij}$	strain rate tensor on the grid level	n	time step $n$
$\overline{S}_{ij}$	strain-rate tensor on the test level	SS	scale-similarity
$T_{ij}$	subgrid-scale stress on the test level	<i>Subscripts</i>	
$u_i$	instantaneous velocity in $i$ direction	$c$	consistent
$u_\tau$	friction velocity		
$x_{\text{max}}, y_{\text{max}}, z_{\text{max}}$	channel length, height and width, respectively		

computational cost involved in solving equations for the dynamic coefficients (Fredholm's integral equation of the second kind) is not justified by more accurate results. Computationally less consuming dynamic procedures are obviously needed to obtain the coefficients in the transport equation for  $k_{\text{sgs}}$ .

This paper presents a mixed dynamic model in which the SGS kinetic energy model is used as a dissipative part in the model. The dynamic models based on the  $k_{\text{sgs}}$  proved to give an accurate representation of the unresolved scales in a coarse LES (Krajnović and Davidson, 2001; Krajnović and Davidson, 1999; Sohankar et al., 2000a,b). They are more robust than the Germano model, (Sohankar et al., 2000a,b) and allow transfer of turbulent energy from small to large scales (backscatter). Furthermore, the velocity scale,  $k_{\text{sgs}}^{1/2}$ , in the mixed models contains some information on the small scales, and the solution of the transport equations for  $k_{\text{sgs}}$  contributes a history effect in the model.

## 2. Formulation of the proposed model

This section presents a new mixed one-equation SGS model and derives the dynamic procedures for the model coefficients. We then summarize the model as it is implemented in the code.

We first give some notations needed for the formulation of the model. The mixed models for the SGS stresses consist of one scale-similarity part and one eddy-viscosity part of the SGS stress tensor,  $\tau_{ij} = \overline{u_i u_j} - \bar{u}_i \bar{u}_j$ . Here, an overbar denotes a grid filter with a filter width  $\Delta$ . If we denote our modeled SGS stress by  $\tau_{ij}^{\text{M}}$ , its scale-similarity part by  $\tau_{ij}^{\text{SS}}$  and the eddy-viscosity part by  $\tau_{ij}^{\text{EV}}$ , then

$$\tau_{ij}^{\text{M}} = \tau_{ij}^{\text{SS}} + \tau_{ij}^{\text{EV}}. \quad (1)$$

The scale-similarity and the eddy-viscosity stresses are defined as

$$\begin{aligned} \tau_{ij}^{\text{SS}} &= \overline{u_i u_j} - \bar{u}_i \bar{u}_j, \\ \tau_{ij}^{\text{EV}} &= -2C(x, y, z, t) \Delta k_{\text{sgs}}^{1/2} \bar{S}_{ij} + \frac{2}{3} \delta_{ij} k_{\text{sgs}}, \end{aligned} \quad (2)$$

where  $C(x, y, z, t)$  is a space and time-dependent coefficient.  $\bar{S}_{ij}$  is the strain rate tensor on the grid level. Instead of using the velocity scale  $|\bar{S}|$ , which is common practice in the dynamic models, we use  $k_{\text{sgs}}^{1/2}$  as the velocity scale. Through  $k_{\text{sgs}}^{1/2}$ , information from the small scales is included in the SGS model. The SGS kinetic energy,  $k_{\text{sgs}}$ , is defined as  $k_{\text{sgs}} = (1/2) \tau_{ii}^{\text{EV}}$ . The coefficient,  $C(x, y, z, t)$ , is computed using a dynamic procedure and, for that, we must define some quantities on the test level. If we introduce  $\hat{\cdot}$  as a test-filter with a filter width of  $\hat{\Delta} = 2\Delta$  the SGS stress on the test level can be written as  $T_{ij} = \overline{\overline{u_i u_j}} - \overline{\hat{u}_i} \overline{\hat{u}_j}$ . Similar to  $\tau_{ij}^{\text{SS}}$  and  $\tau_{ij}^{\text{EV}}$ ,  $T_{ij}^{\text{SS}}$  and

$T_{ij}^{EV}$  are introduced as the scale-similarity and the eddy-viscosity parts of the modeled SGS stress on the test level,  $T_{ij}^M$ , i.e.

$$T_{ij}^M = T_{ij}^{SS} + T_{ij}^{EV}. \quad (3)$$

$T_{ij}^{SS}$  and  $T_{ij}^{EV}$  are modeled as

$$T_{ij}^{SS} = \overline{\overline{\bar{u}_i \bar{u}_j}} - \overline{\bar{u}_i} \overline{\bar{u}_j}, \quad (4)$$

$$T_{ij}^{EV} = -2C(x, y, z, t) \Delta K^{1/2} \widehat{\bar{S}}_{ij} + \frac{2}{3} \delta_{ij} K,$$

where the strain-rate tensor on the test level,  $\widehat{\bar{S}}_{ij}$ , is defined as

$$\widehat{\bar{S}}_{ij} = \frac{1}{2} \left( \frac{\partial \overline{\bar{u}}_i}{\partial x_j} + \frac{\partial \overline{\bar{u}}_j}{\partial x_i} \right). \quad (5)$$

The SGS kinetic energy on test level,  $K$ , is defined as  $K = (1/2) T_{ii}^{EV}$ . The eddy-viscosity part,  $\Pi_{k_{sgs}}$ , and the scale-similarity part,  $\Pi^{SS}$ , of the SGS dissipation of the resolved kinetic energy are defined as

$$\Pi_{k_{sgs}} = -\tau_{ij}^{EV} \bar{S}_{ij}, \quad \Pi^{SS} = -\tau_{ij}^{SS} \bar{S}_{ij}. \quad (6)$$

The SGS kinetic energy,  $k_{sgs}$ , is obtained from the modeled transport equation (for the derivation of the  $k_{sgs}$  equation, see Appendix A),

$$\frac{\partial k_{sgs}}{\partial t} + \frac{\partial}{\partial x_j} (\bar{u}_j k_{sgs}) = \Pi_{k_{sgs}} + \frac{\partial}{\partial x_j} \left\{ (v_{sgs} + \nu) \frac{\partial k_{sgs}}{\partial x_j} \right\} - C_\epsilon \frac{k_{sgs}^{3/2}}{\Delta} + \Pi^{SS} + \nu \frac{\partial^2}{\partial x_j \partial x_j} \left( \frac{1}{2} \tau_{ii}^{SS} \right) - \frac{\partial}{\partial t} \left( \frac{1}{2} \tau_{ii}^{SS} \right) - \frac{\partial}{\partial x_j} \left\{ \frac{1}{2} \tau_{ii}^{SS} \bar{u}_j \right\}. \quad (7)$$

A homogeneous coefficient,  $C_{hom}(t)$ , is used in the definition of the SGS turbulent viscosity,  $\nu_{sgs}$ , as

$$\nu_{sgs} = C_{hom}(t) \Delta k_{sgs}^{1/2} \quad (8)$$

in Eq. (7) and in the momentum equations. The reason why a homogeneous coefficient is used is that the local coefficient  $C(x, y, z, t)$  yields a highly oscillating eddy viscosity field including a significant partition with negative values, which is destabilizing in numerical simulations.  $C_{hom}(t)$  is computed with the requirement that the SGS dissipation of the resolved kinetic energy in the whole computational domain remains the same as with the local coefficient  $C(x, y, z, t)$ , i.e.

$$\left\langle 2C(x, y, z, t) \Delta k_{sgs}^{1/2} \bar{S}_{ij} \bar{S}_{ij} \right\rangle_{xyz} = 2C_{hom}(t) \left\langle \Delta k_{sgs}^{1/2} \bar{S}_{ij} \bar{S}_{ij} \right\rangle_{xyz}, \quad (9)$$

where  $\langle \cdot \rangle_{xyz}$  denotes space averaging over the entire domain.

We now use the Germano identity, i.e.

$$L_{ij} = T_{ij} - \widehat{\tau}_{ij}, \quad (10)$$

where the resolved stress,  $L_{ij}$ , is

$$L_{ij} = \overline{\overline{\bar{u}_i \bar{u}_j}} - \overline{\bar{u}_i} \overline{\bar{u}_j}. \quad (11)$$

By substituting modeled stresses from Eqs. (1)–(4) into Eq. (10) we have

$$L_{ij} - H_{ij} = 2C(x, y, z, t) M_{ij}, \quad (12)$$

where

$$H_{ij} = \left( \overline{\overline{\bar{u}_i \bar{u}_j}} - \overline{\bar{u}_i} \overline{\bar{u}_j} \right), \quad (13)$$

$$M_{ij} = \Delta \overline{\overline{k_{sgs}^{1/2} \bar{S}_{ij}}} - \Delta K^{1/2} \widehat{\bar{S}}_{ij}. \quad (14)$$

The square error,  $E_{ij} E_{ij} = (L_{ij} - H_{ij} - 2C(x, y, z, t) M_{ij})^2$ , is minimized (Lilly, 1992) to obtain

$$C(x, y, z, t) = \frac{(L_{ij} - H_{ij}) M_{ij}}{2M_{ij} M_{ij}}. \quad (15)$$

Taking the trace of the Germano identity in Eq. (10) and using the definitions of the SGS kinetic energy on the grid filter level,  $k_{sgs}$ , and on the test filter level,  $K$ , we can compute the test level kinetic energy as

$$K = \widehat{k_{sgs}} + \frac{1}{2} (L_{ii} - H_{ii}). \quad (16)$$

In RANS, Rodi (1976) proposed that the convective and diffusive transport of  $\overline{\bar{u}_i \bar{u}_j}$  are proportional to that of  $k$  with the proportionality coefficient  $\overline{\bar{u}_i \bar{u}_j} / k$ . Here we use a similar assumption when computing the dissipation coefficient,  $C_\epsilon$ , in Eq. (7). We assume that the convective and diffusive transport of  $k_{sgs}$  are proportional to that of  $K$  with the proportionality coefficient  $k_{sgs} / K$ . Since

$$C_K + D_K = \Pi_K + \Pi_K^{SS} - \epsilon_K,$$

$$\widehat{C}_{k_{sgs}} + \widehat{D}_{k_{sgs}} = \widehat{\Pi}_{k_{sgs}} + \widehat{\Pi^{SS}} - \widehat{\epsilon}_{k_{sgs}},$$

with the convection terms  $C_K$  and  $C_{k_{sgs}}$  and the diffusion terms  $D_K$  and  $D_{k_{sgs}}$ , we obtain (note that the scale-similarity terms have been absorbed in the convection and diffusion terms)

$$\frac{k_{sgs}}{K} (\Pi_K + \Pi_K^{SS} - \epsilon_K) = \widehat{\Pi}_{k_{sgs}} + \widehat{\Pi^{SS}} - \widehat{\epsilon}_{k_{sgs}}, \quad (17)$$

where

$$\Pi_K = -T_{ij}^{EV} \widehat{\bar{S}}_{ij}, \quad \Pi_K^{SS} = -T_{ij}^{SS} \widehat{\bar{S}}_{ij},$$

$$\epsilon_K = C_\epsilon \frac{K^{3/2}}{\Delta}, \quad \epsilon_{k_{sgs}} = C_\epsilon \frac{k_{sgs}^{3/2}}{\Delta}. \quad (18)$$

This gives

$$C_\epsilon^{n+1} = \left[ \Pi_K + \Pi_K^{SS} - \frac{K}{k_{sgs}} \left( \widehat{\Pi}_{k_{sgs}} + \widehat{\Pi^{SS}} - C_\epsilon^n \frac{k_{sgs}^{3/2}}{\Delta} \right) \right] \frac{\Delta}{K^{3/2}}, \quad (19)$$

where  $C_\epsilon^{n+1}$  denotes the dissipation coefficient for time step  $n + 1$ . Since the viscous dissipation must be non-negative by definition,  $C_\epsilon$  is constrained as  $C_\epsilon \geq 0$ .

The new mixed one-equation SGS model can be summarized as follows:

1. The modeled transport equation (Eq. (7)) for the sub-grid kinetic energy  $k_{\text{sgs}}$  is solved.
2. The eddy-viscosity and the scale-similarity parts of the SGS dissipation of the resolved kinetic energy in Eq. (6) are computed. When computing the eddy-viscosity part of the SGS dissipation of the resolved kinetic energy, the local dynamic coefficient (Eq. (15)) is used in the expression for the eddy-viscosity stress in Eq. (2).
3. The local dynamic dissipation coefficient is computed from Eq. (19).
4. The eddy-viscosity part of the subgrid stresses in the momentum equation is computed using a homogeneous coefficient,  $C_{\text{hom}}(t)$ .  $C_{\text{hom}}(t)$  is also used in the diffusion term in the modeled  $k_{\text{sgs}}$  equation.
5. The nodes adjacent to the wall are located in the viscous sublayer and thus the boundary condition for the subgrid kinetic energy is  $k_{\text{sgs}} = 0$  at all walls.

### 2.1. Numerical method

An implicit finite-volume method is used for solving the incompressible Navier–Stokes equations on non-staggered grids (Davidson, 2001; Emvin, 1997). Both convective and viscous plus subgrid fluxes are approximated by central differences of second-order accuracy. A Crank–Nicolson second-order scheme was used for time integration. Although no explicit dissipation is added to prevent odd–even decoupling, an implicit dissipation is present. This is done by adding the difference between the pressure gradient at the face and the node. It can be shown that this term is proportional to the third derivative of pressure, i.e.  $\partial^3 p / \partial x_i^3$ . This term corresponds to Rhie–Chow dissipation (Rhie and Chow, 1983). Details about this code are given in Davidson (2001).

This work uses the top-hat filter. The grid filtering is applied implicitly through the discretization. The explicit filtering at the test level is done numerically by integrating over the test cell assuming linear variation of the variables (Zang et al., 1993), i.e. (see Fig. 1)

$$\begin{aligned} \overline{\bar{u}}_{I,J,K} = & \frac{1}{8} (\bar{u}_{I-1/2,J-1/2,K-1/2} \\ & + \bar{u}_{I+1/2,J-1/2,K-1/2} + \bar{u}_{I-1/2,J+1/2,K-1/2} \\ & + \bar{u}_{I+1/2,J+1/2,K-1/2} + \bar{u}_{I-1/2,J-1/2,K+1/2} \\ & + \bar{u}_{I+1/2,J-1/2,K+1/2} + \bar{u}_{I-1/2,J+1/2,K+1/2} \\ & + \bar{u}_{I+1/2,J+1/2,K+1/2}). \end{aligned} \quad (20)$$

The source terms in the numerical solution of Eq. (7) are discretized as  $S = S_p k_{\text{sgs}} + S_u$  with  $S_p = \min(b)/k_{\text{sgs}}$  and  $S_u = \max(b)$ . Here,  $b$  is the scale-similarity terms and the eddy-viscosity production and dissipation terms in Eq. (7).

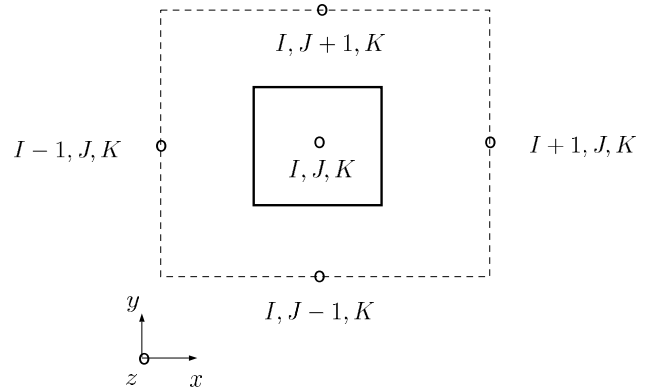


Fig. 1. Grid filtering volume (solid line) and test filtering volume (dashed line).

## 3. Results

The mixed one-equation model was first applied to the simple case of the flow in a plane channel. Despite its simplicity, this flow is sensitive to the choice of model and can expose problems in a model. It is a standard test case for new models and, at a relatively low Reynolds number ( $Re_\tau = 395$ ), an accurate prediction of this flow is probably a minimum requirement for a model.

Although the model may work for the channel flow simulation, our main object was to evaluate the model in a fully inhomogeneous recirculation flow. The model was thus applied to the flow around a surface-mounted cube. This flow is fully inhomogeneous with multiple recirculations.

### 3.1. Channel flow

We simulated the flow in a plane channel with  $Re_\tau = 395$ . The computational domain is  $x_{\text{max}} = 2\pi\delta$ ,  $y_{\text{max}} = 2\delta$  and  $z_{\text{max}} = \pi\delta$  ( $\delta$  being the half channel height) and the mesh is  $64 \times 64 \times 64$  cells. Periodic boundary conditions were used in the stream-wise and span-wise directions. No-slip conditions were used at the solid walls. The homogeneous Neumann condition was used for the pressure at the walls. The grid was stretched in the wall-normal direction and thus the implicit filter was also non-uniform. It is well known that for the non-uniform filters a filtering operation and the spatial differentiation do not commute, see Ghosal and Moin (1995). It is practice in LES of channel flows to filter only in the stream-wise and the span-wise directions, thus avoiding difficulties with the commutation error. In more complex geometries, the grids are non-uniform in all directions and filtering is performed in all directions. To test the model under the same conditions in both the channel flow and the cube simulations, we also filtered in the wall-normal direction in the channel flow LES. Such a

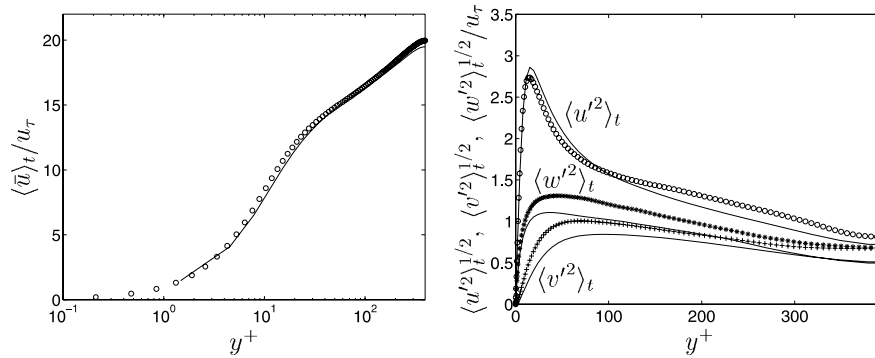


Fig. 2. Channel flow with  $Re_\tau = 395$ ,  $C_{SS} = 0.2$ . Comparison of mixed one-equation model (solid line) and DNS data (symbols).

simulation gives a more fair picture of the model performance in complex geometries.

The mean velocity and the RMS fluctuations are compared with DNS data of Kim et al. (1987). We find good agreement between our LES and the DNS in Fig. 2.

### 3.2. Flow around a surface-mounted cube

In this section we present LES of the flow around a surface-mounted cube placed on a channel wall at  $Re = 40000$ , based on the incoming mean bulk velocity and the cube height. The flow is complex and has massive separations (Krajnović and Davidson, 2001). The geometry of the computational domain is given in Fig. 3. A domain with an upstream length of  $x_1/H = 3$  and a downstream length of  $x_2/H = 6$  was used for the simulation, while the span-wise width was set to  $b/H = 7$  (see Fig. 3). The experimental profile (constant in time) was used at the inlet in this work. The lateral boundaries were treated as slip surfaces using the symmetry conditions  $\partial \bar{u} / \partial z = \partial \bar{v} / \partial z = \bar{w} = 0$ . At the downstream boundary, the convective boundary condition  $\partial \bar{u}_i / \partial t + U_c (\partial \bar{u}_i / \partial x) = 0$  was used. Here,  $U_c$  was set equal to the mean bulk velocity,  $U_b$ . No-slip conditions were used at the solid walls. The homogeneous Neumann condition was used for the pressure at all boundaries. A computational mesh of  $82 \times 50 \times 66$  nodes was used. Near the walls of the channel,  $y_{\min}^+ = 3.7$ , while  $y_{\min}^+ = 5.2$  on the top of the cube. Such a coarse resolution implies that a significant fraction of the turbulent energy is modeled. Thus the model has a large influence on the resulting statistics.

A series of time-averaged velocities and turbulent stresses are compared with the experiments of Martinuzzi and Tropea (1993) (see Figs. 4–6). The separation region at the top of the cube is in good agreement with the experiments (see Fig. 4). There is some difference between experimental and LES velocity profiles at positions  $x/H = 0.75$ ,  $x/H = 1.08$  and  $x/H = 2.0$ , but the results are still fairly accurate. The difference becomes

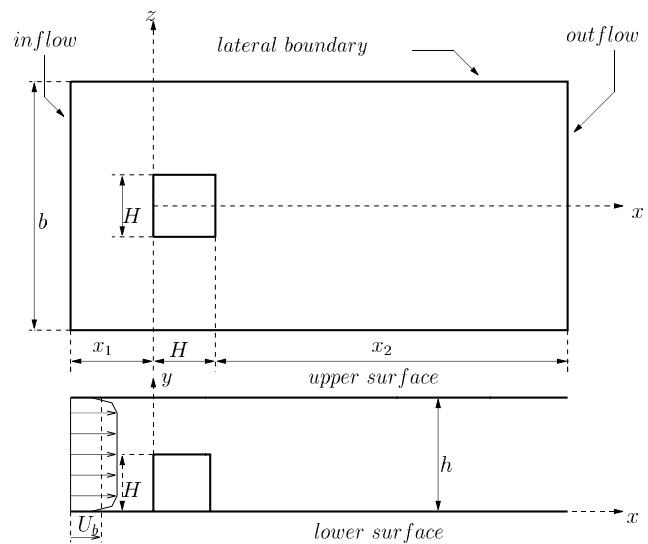


Fig. 3. Surface-mounted cube. Geometry of the computational domain.

insignificant as we move further downstream. The resolved Reynolds stresses shown in Figs. 5 and 6 are in somewhat poorer agreement with the experiments than are the velocities, but the results are still fairly accurate. The time history of the homogeneous dynamic coefficient,  $C_{\text{hom}}$ , is shown in Fig. 7. The time-averaged mean value is approximately 2.5 times lower than in the eddy-viscosity one-equation model of Davidson (1997), see Krajnović and Davidson (1999).

## 4. Mathematical consistency and computational cost

The importance of expressing the SGS stress tensor on test level,  $T_{ij}$ , entirely in the test-level velocity,  $\overline{u_i}$ , was addressed in Vreman et al. (1994a). According to these authors, the modeled  $T_{ij}$  should, in order to be mathematically consistent, be expressed entirely in  $\overline{u_i}$ . Here, we have replaced the model in Eq. (4) by the expression

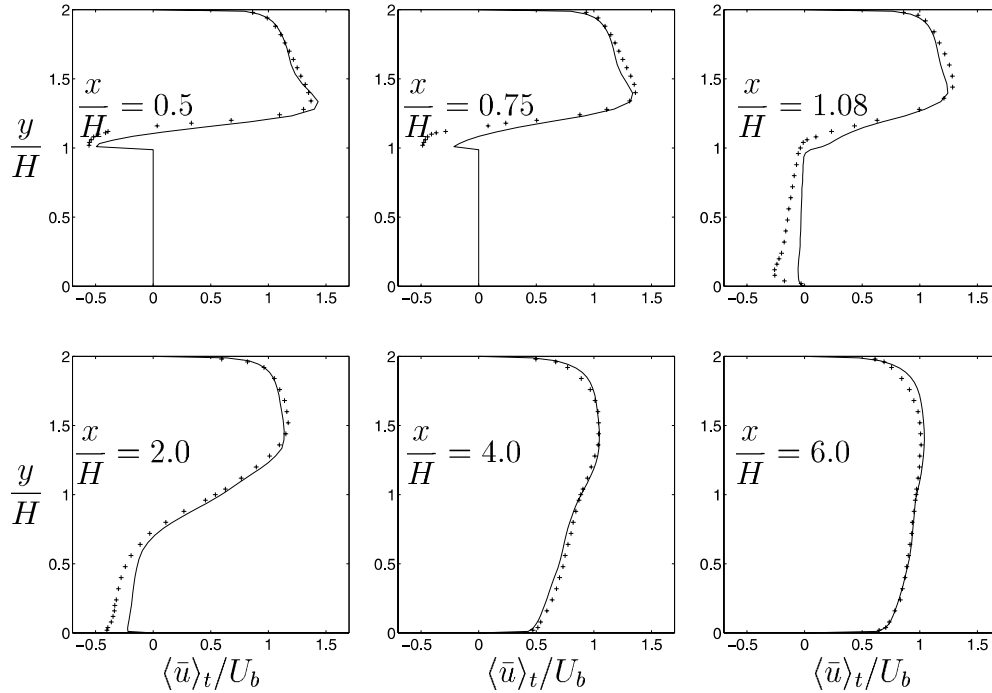


Fig. 4. Surface-mounted cube. Comparison of mixed one-equation model (solid line) and experiments (symbols).

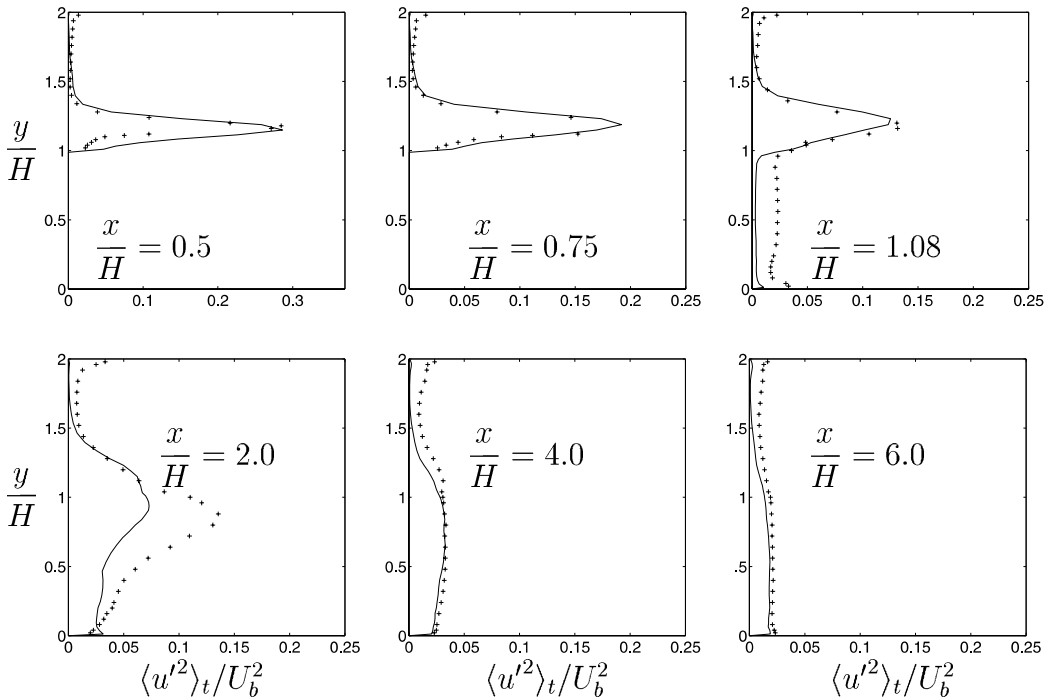


Fig. 5. Surface-mounted cube. Resolved stresses. Comparison of mixed one-equation model (solid line) and experiments (symbols).

$$T_{ijc}^{SS} = \overline{\overline{\bar{u}_i \bar{u}_j}} - \overline{\overline{\bar{u}_i}} \overline{\overline{\bar{u}_j}} \quad (21)$$

proposed by Vreman et al. (1994a) and obtained

$$H_{ijc} = \overline{\overline{\bar{u}_i \bar{u}_j}} - \overline{\overline{\bar{u}_i}} \overline{\overline{\bar{u}_j}} - (\overline{\overline{\bar{u}_i \bar{u}_j}} - \overline{\overline{\bar{u}_i}} \overline{\overline{\bar{u}_j}}) \quad (22)$$

instead of Eq. (13). Subscript ‘c’ in Eqs. (21) and (22) denotes consistency. In the simulations we find that  $H_{ij}$  obtained from Eq. (13) is larger than  $H_{ijc}$ . This gives a larger magnitude of  $C$  when Eq. (22) is used. The same observation was also made by Vreman et al. (1994a). They noted that  $\bar{u}_i$  contains more small-scale structures than  $\overline{\overline{\bar{u}_i}}$  and therefore  $H_{ij}$  is larger than  $H_{ijc}$ . We

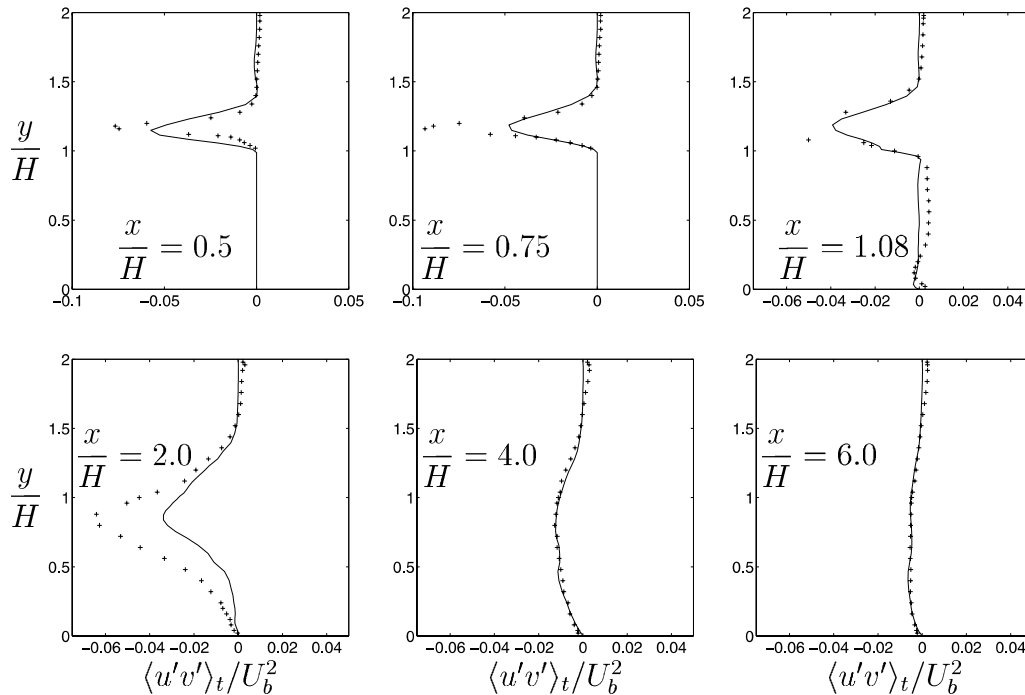


Fig. 6. Surface-mounted cube. Resolved stresses. Comparison of mixed one-equation model (solid line) and experiments (symbols).

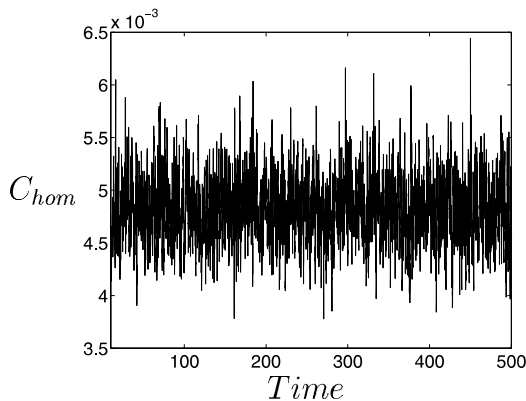


Fig. 7. Surface-mounted cube. Time history of the dynamic coefficient  $C_{hom}$ .

compared the models in Eqs. (13) and (22) and found very little difference in the results for the two test cases presented in this paper. The mathematically consistent model increased the computational cost by some 5% owing to the extra filtering. This suggests the use of the basic model from Eq. (4). However, a more important reason to use Eq. (13) rather than Eq. (22) is that the implementation of Eq. (13) is much less complicated.

The computational cost is of course dependent on the implementation (programming and parallelization) and on the machine used in the simulation. This work used SGI R10000 CPUs. The solution of the  $k_{sgs}$  equation and the dynamic procedure increases the computational cost by some 18% in the case of the surface-mounted cube as compared to when the Smagorinsky model is

used. Carati et al. (1995) reported that the one-equation model of Ghosal et al. (1995) required 67% more CPU time than the standard Smagorinsky model.

## 5. Proper dissipation

The problem of insufficient model dissipation when using the dynamic mixed models is little discussed in the literature. This problem occurs because the eddy-viscosity part of the model becomes too small and does not produce enough dissipation. This is especially the case when an energy conservative scheme such as the central differencing scheme is used for the discretization.

Zang et al. (1993) implemented a dynamic mixed model which was applied to the simulations of recirculating flows. In addition to the SGS dissipation from the eddy-viscosity part of the model, some numerical dissipation is present owing to the use of some upwinding in the convection terms in their code (Sarghini and Piomelli, 1999; Meneveau and Katz, 2000). This upwinding reduces both the numerical and the physical oscillations.

Ribault et al. (1999) introduced a damping on the similarity part of the model in large-eddy simulation of a plane jet using the dynamic mixed model (Zang et al., 1993; Vreman et al., 1994a). Damping the similarity part of the model increases the relative importance of the dissipative part,  $\tau_{ij}^{EV}$ , thereby stabilizing the computation. We introduced this damping through the damping coefficient,  $C_{SS}$ , in the expression for the subgrid stress model on the grid level,

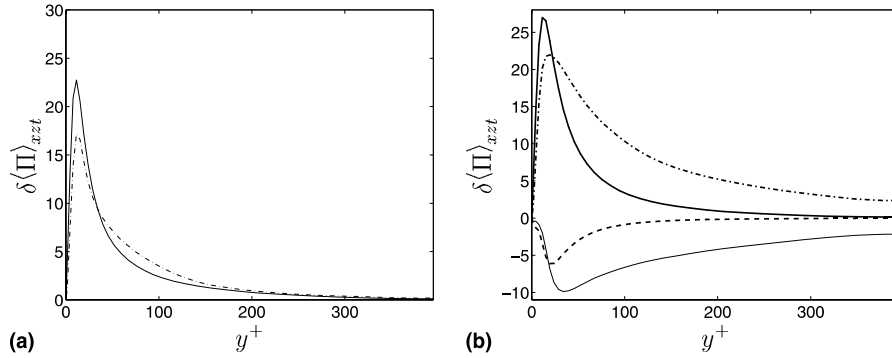


Fig. 8. Channel flow with  $Re_\tau = 395$ . (a) Dissipation:  $\delta \langle \Pi \rangle_{xzt}$  (solid line);  $\delta \langle \Pi^{EV} \rangle_{xzt}$  (dashed-dotted line); (b) dissipation:  $\delta \langle \Pi^{SS} \rangle_{xzt}$  (solid line);  $\delta \langle \Pi^{SS^-} \rangle_{xzt}$  (dashed line);  $\delta \langle \Pi^{EV} \rangle_{xzt}$  (dashed-dotted line);  $\delta \langle \Pi^{EV} \rangle_{xzt}$  (thin solid line).

$$\tau_{ij}^{SS} = C_{SS} (\overline{\bar{u}_i \bar{u}_j} - \bar{u}_i \bar{u}_j) \quad (23)$$

(Liu et al., 1994), and on the test level,

$$T_{ij}^{SS} = C_{SS} (\overline{\bar{u}_i \bar{u}_j} - \bar{u}_i \bar{u}_j), \quad (24)$$

in the momentum equations. Here, we have assumed the scale invariance and used the same coefficient ( $C_{SS}$ ) at the grid-filtered level and the test-filtered level. This coefficient should have a magnitude between 0 and 1.  $C_{SS} = 0.2$  was used for the channel flow simulation, giving some improvement in the results. The results of the cube simulation were almost unchanged when damping was introduced. The scale-similarity stress in Eq. (2) is Galilean invariant, see Germano (1986), and thus  $C_{SS}$  can be chosen arbitrarily between 0 and 1.

## 6. Turbulent energy transport

It was found in Domaradzki et al. (1993, 1994) that the SGS energy transfer is a local phenomenon caused by the interaction of the scales immediately above the cut-off with those immediately below it. We expect the scale-similarity part of the SGS stresses to give a correct representation of this interaction. The non-local transfer of energy is represented by the eddy-viscosity part of the model.

The transfer of the turbulent energy takes place through the dissipation term,  $\Pi = -\tau_{ij}(\partial \bar{u}_i / \partial x_j)$ , in the equation for the resolved kinetic energy

$$\begin{aligned} \frac{\partial \bar{k}}{\partial t} + \frac{\partial}{\partial x_j} (\bar{u}_j \bar{k}) = & -\frac{1}{\rho} \frac{\partial}{\partial x_i} (\bar{u}_i \bar{p}) + \frac{\partial}{\partial x_j} \left( v \frac{\partial \bar{k}}{\partial x_j} \right) \\ & - \frac{\partial}{\partial x_j} (\bar{u}_i \tau_{ij}) - v \frac{\partial \bar{u}_i}{\partial x_j} \frac{\partial \bar{u}_i}{\partial x_j} - \Pi. \end{aligned} \quad (25)$$

The term  $\Pi = \Pi_{k_{sgs}} + \Pi^{SS}$  appears in the equation for  $k_{sgs}$  (Eq. (7)) as a production term. Sarghini and Piomelli (1999) found that the similarity term contributes to

about half of the SGS dissipation  $\Pi$  in channel flow simulations. The mixed one-equation model gives the same results except at  $y^+ \approx 15$ , where the scale-similar part of  $\langle \Pi \rangle_{xzt}$  is some 20% larger than the eddy-viscosity part (see Fig. 8(a)).

The SGS dissipation  $\Pi$  is positive in the mean (see Fig. 8(a)) although there is local backscatter, i.e. transfer of the turbulent energy from small to resolved scales (see Fig. 8(b)). The backward and the forward scatter components of  $\Pi$ , respectively denoted  $\Pi^-$  and  $\Pi^+$ , are computed as

$$\Pi^- = \frac{1}{2}(\Pi - |\Pi|), \quad (26)$$

$$\Pi^+ = \frac{1}{2}(\Pi + |\Pi|). \quad (27)$$

In a study of the reverse flow of energy, Krajnović and Davidson (1999, 2001) computed the SGS dissipation of the resolved kinetic energy,  $\Pi_{k_{sgs}} = -\tau_{ij} \bar{S}_{ij}$ , in the one-equation models of Davidson (1997) and Menon and Kim (1996). It was found that the strongest backscatter occurs near the front corners of the cube. It was also found in simulations by Sohankar et al. (2000a,b) of the flow around a square cylinder that strong backscatter occurs near the front corners.

In the present paper, we studied both the eddy-viscosity,  $\Pi_{k_{sgs}} = -\tau_{ij}^{EV} \bar{S}_{ij}$ , and the scale-similarity part of the SGS dissipation of the resolved kinetic energy,  $\Pi^{SS} = -\tau_{ij}^{SS} \bar{S}_{ij}$ , in Eq. (7). Also here we found the strongest backscatter near the front corners. We find that the scale-similarity forward scatter is larger than the eddy-viscosity one. The eddy-viscosity backward scatter is slightly larger than the scale-similarity backward scatter (see Fig. 9).

## 7. Properties of the model

The modeled SGS stresses must satisfy the same properties as the exact ones. These properties are dis-

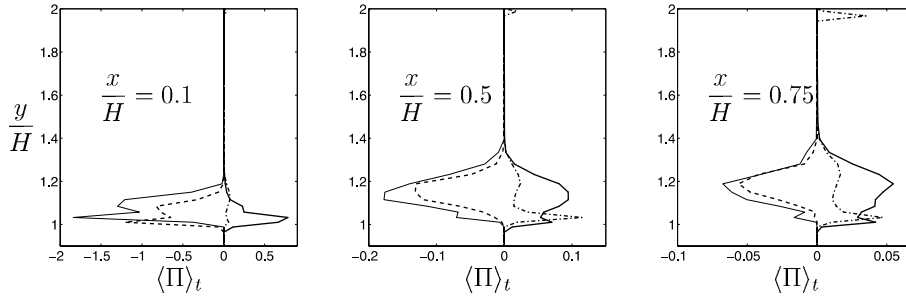


Fig. 9. Surface-mounted cube. Dissipation:  $\langle \Pi^{SS^+} \rangle_t$  (solid line);  $\langle \Pi^{SS^-} \rangle_t$  (dashed line);  $\langle \Pi^{EV^+} \rangle_t$  (dashed-dotted line);  $\langle \Pi^{EV^-} \rangle_t$  (thin solid line).

cussed in Fureby and Tabor (1997) and Ghosal (1999). It is trivial to supply mathematical proof for some of the properties and very difficult for others (e.g. the realizability of one-equation models). This section discusses the most important properties of the mixed one-equation model.

### 7.1. Galilean invariance

According to Speziale (1985), the basic physics of the turbulence requires that the description of turbulence is the same in all inertial frames of reference. This requirement is satisfied if the SGS stress model is invariant under the Galilean transformation.  $\tau_{ij}^{SS}$  in Eq. (2) is defined using the redefinition of the turbulent stresses according to Germano (1986) and thus is Galilean invariant. The diffusion term,

$$\frac{\partial}{\partial x_j} \left\{ (v_{sgs} + \nu) \frac{\partial k_{sgs}}{\partial x_j} \right\},$$

in the equation for the SGS kinetic energy (Eq. (7)) is Galilean invariant. The sum of the transient and convective term,

$$\frac{\partial}{\partial t} (\tau_{ii}^{SS}) + \frac{\partial}{\partial x_j} (\tau_{ii}^{SS} \bar{u}_j),$$

is Galilean invariant, making the entire equation Galilean invariant. The Galilean invariance of the resolved stresses,  $L_{ij}$ , and the quantities on the test level,  $K$  and  $\bar{S}_{ij}$ , follows from Eqs. (11), (16) and (5). Using these results in Eq. (15), it can be shown that the dynamic coefficient,  $C$ , is Galilean invariant. The invariance of the model now follows from Eqs. (2) and (1).

### 7.2. Realizability

If the model violates the realizability condition, it may give unphysical solutions. These conditions have earlier been described for the SGS stress tensor by

Vreman et al. (1994b) and Ghosal (1999). The realizability conditions are given by the following two inequalities:

$$(i) \quad \tau_{ii} \geq 0 \tag{28}$$

with no summation on  $i$ .

$$(ii) \quad |\tau_{ij}| \leq (\tau_{ii} \tau_{jj})^{1/2} \quad \forall i \neq j \tag{29}$$

with no summation on  $i$  and  $j$ . Here we present the realizability conditions for the mixed one-equation SGS model.

The first realizability condition is fulfilled if

$$\tau_{ii}^M = \tau_{ii}^{SS} + \tau_{ii}^{EV} \geq 0 \tag{30}$$

i.e.

$$\frac{1}{2\Delta k_{sgs}^{1/2} \bar{S}_{33}} (\tau_{33}^{SS} + \frac{2}{3} k_{sgs}) \leq C \leq \frac{1}{2\Delta k_{sgs}^{1/2} \bar{S}_{11}} (\tau_{11}^{SS} + \frac{2}{3} k_{sgs}). \tag{31}$$

Here we assume that

$$\bar{S}_{33} = \min_i (\bar{S}_{ii}) \leq 0, \quad \bar{S}_{11} = \max_i (\bar{S}_{ii}) \geq 0.$$

The second realizability condition is fulfilled if

$$|\tau_{ij}^{SS} + \tau_{ij}^{EV}| \leq \left\{ (\tau_{ii}^{SS} + \tau_{ii}^{EV})(\tau_{jj}^{SS} + \tau_{jj}^{EV}) \right\}^{1/2} \tag{32}$$

i.e.

$$\frac{-\beta}{2\alpha} - \frac{(\beta^2 - 4\alpha\gamma)^{1/2}}{2\alpha} \leq C \leq \frac{-\beta}{2\alpha} + \frac{(\beta^2 - 4\alpha\gamma)^{1/2}}{2\alpha} \tag{33}$$

with

$$\alpha = 4\Delta^2 k_{sgs} (\bar{S}_{ij}^2 - \bar{S}_{ii} \bar{S}_{jj}), \tag{34}$$

$$\beta = 2\Delta k_{sgs}^{1/2} (\tau_{ii}^{SS} \bar{S}_{jj} + \tau_{jj}^{SS} \bar{S}_{ii} - 2\tau_{ij}^{SS} \bar{S}_{ij}) + \frac{4}{3} \Delta k_{sgs}^{3/2} (\bar{S}_{ii} + \bar{S}_{jj}), \tag{35}$$

$$\gamma = -\tau_{ii}^{SS} \tau_{jj}^{SS} - \frac{2}{3} k_{sgs} (\tau_{ii}^{SS} + \tau_{jj}^{SS}) - \frac{4}{9} k_{sgs}^2 + (\tau_{ij}^{SS})^2. \quad (36)$$

The bounds on  $C$  following from Eqs. (31) and (33) ensure that  $k_{sgs} \geq 0$ . It was found for both test cases studied in this paper that at least 99% of the grid points satisfy both realizability conditions in Eqs. (31) and (33) at every time step during the entire simulation. The corresponding number of points in the model by Ghosal et al. (1995) was 95% for the first realizability condition, when they simulated for the experiment of decaying isotropic turbulence of Comte-Bellot and Corrsin (1971).

A positive filter function like the top-hat filter and the Gaussian filter is a necessary requirement for realizability (Vreman et al., 1994b). As already mentioned, we used the top-hat filter. It was found in Vreman et al. (1994b) that  $k_{sgs}$  was negative in many regions of the flow when a spectral cut-off filter, which is non-positive, was used. Moreover, the correlation between  $\tau_{ij}^{SS}$  and  $\tau_{ij}$  decreases to almost zero when a spectral cut-off filter is used, see Liu et al. (1994). For these reasons, positive filters should be used together with the mixed one-equation model.

### 7.3. Near-wall behavior

The exact SGS stresses behave close to the wall such that:  $\tau_{11} \sim y^2$ ,  $\tau_{22} \sim y^4$ ,  $\tau_{33} \sim y^2$ ,  $\tau_{12} \sim y^3$ ,  $\tau_{13} \sim y^2$  and  $\tau_{23} \sim y^3$ . Near the wall

$$\bar{u}_1 \sim y, \quad \bar{u}_2 \sim y^2, \quad \bar{u}_3 \sim y. \quad (37)$$

Thus the scale-similarity part of the SGS stresses in Eq. (2) displays the correct behavior near the wall. In the computation of the eddy-viscosity part in Eq. (2), the homogeneous coefficient  $C_{hom}(t) \sim y^0$  is used. Obviously the SGS viscosity exhibits behavior different from  $y^3$  close to the wall. This is less important because the magnitude of the scale-similarity part of the stresses is large close to the wall. For  $C_{SS} = 0.2$  used in Eq. (23), some 50% of the total SGS stress is carried by the scale-similarity part of the model. This means that the modeled SGS stress  $\tau_{ij}^M$  has approximately the correct behavior near the wall.

### 7.4. Dynamic coefficients

As already mentioned, a homogeneous coefficient  $C_{hom}(t)$  is used in the diffusion term of the  $k_{sgs}$  equation and in the momentum equations for stability reasons. Here we consider the influence of the increase of the computational domain on the  $C_{hom}(t)$ . From Eq. (9) follows

$$C_{hom}(t) = \frac{\left\langle 2C(x, y, z, t) \Delta k_{sgs}^{1/2} \bar{\mathcal{S}}_{ij} \bar{\mathcal{S}}_{ij} \right\rangle_{xyz}}{2 \left\langle \Delta k_{sgs}^{1/2} \bar{\mathcal{S}}_{ij} \bar{\mathcal{S}}_{ij} \right\rangle_{xyz}}. \quad (38)$$

There are three main cases:

1. An increase of the domain in the laminar far-field flow will not influence the homogeneous coefficient  $C_{hom}(t)$  in Eq. (38) because  $k_{sgs} = 0$  in the laminar part of the domain.
2. A change of the volume of homogeneous flow, e.g. a channel flow with periodic boundary conditions, from e.g.  $V_1$  to  $V_2$  will only lead to multiplication on the numerator and the denominator in Eq. (38) with  $V_2/V_1$  and thus not change the value of  $C_{hom}(t)$ .
3. In case of inhomogeneous flow, e.g. flow around a surface-mounted cube, the homogeneous coefficient  $C_{hom}(t)$  in Eq. (38) is weakly dependent on the size of the computational domain.

The dissipation coefficient,  $C_\epsilon$  is constrained as  $C_\epsilon \geq 0$ . It was found that in the case of a channel flow negative  $C_\epsilon$  occurred in some 40% of the nodes. These nodes were concentrated around the symmetry line of the channel, i.e. in the low turbulent part, which does not have any large impact on the results.

## 8. Conclusions

A new mixed one-equation SGS model is presented. This model is constructed following the observation that the transfer of turbulent energy is a local process that occurs between the scales closest to the cut-off. The history effects are built into the model through the transport equation for the SGS kinetic energy. The dynamic procedure in the new model is computationally much cheaper than the one used in the model of Ghosal et al. (1995).

Accurate results are obtained in the simulation of the channel flow with  $Re_\tau = 395$  and the flow around a surface-mounted cube with the bulk velocity Reynolds number  $Re = 40000$ . Both mathematically consistent and inconsistent models for  $T_{ij}^{SS}$  were tested. It was found that they give very similar results. The former gives slightly better results with an increase in the computational cost of some 5% in the case of a surface-mounted cube. The scale-similarity part of the SGS stresses on both the grid and the test levels is larger than the eddy-viscosity part. This reduces the significance of the incorrect assumption that the SGS stress is aligned with the resolved strain rate in the eddy-viscosity part of the model.

## Acknowledgements

This work was supported by NUTEK and Volvo Car Corporation. Computer time on the SGI ORIGIN 2000 machines, provided by UNICC at Chalmers, is gratefully acknowledged.

**Appendix A. Derivation of the  $k_{\text{sgs}}$  equation for the mixed one-equation model**

Let us consider Navier–Stokes equations (Eq. (A.1)) and the filtered Navier–Stokes equations (Eq. (A.2))

$$\frac{\partial u_i}{\partial t} + \frac{\partial}{\partial x_j} (u_i u_j) = -\frac{1}{\rho} \frac{\partial p}{\partial x_i} + \nu \frac{\partial^2 u_i}{\partial x_j \partial x_j}, \quad (\text{A.1})$$

$$\frac{\partial \bar{u}_i}{\partial t} + \frac{\partial}{\partial x_j} (\bar{u}_i \bar{u}_j) = -\frac{1}{\rho} \frac{\partial \bar{p}}{\partial x_i} + \nu \frac{\partial^2 \bar{u}_i}{\partial x_j \partial x_j} - \frac{\partial \tau_{ij}}{\partial x_j}, \quad (\text{A.2})$$

where the SGS stress tensor,

$$\tau_{ij} = \overline{u_i u_j} - \bar{u}_i \bar{u}_j \quad (\text{A.3})$$

is modeled as

$$\tau_{ij}^M = \tau_{ij}^{SS} + \tau_{ij}^{EV}. \quad (\text{A.4})$$

Here, the scale-similarity part of the SGS stress tensor is modeled as

$$\tau_{ij}^{SS} = \overline{u_i u_j} - \bar{u}_i \bar{u}_j \quad (\text{A.5})$$

and the eddy-viscosity part is modeled as

$$\tau_{ij}^{EV} = -2C(x, y, z, t) \Delta k_{\text{sgs}}^{1/2} \bar{S}_{ij} + \frac{2}{3} \delta_{ij} k_{\text{sgs}}. \quad (\text{A.6})$$

Now we subtract the product of  $\bar{u}_i$  and Eq. (A.2) from the filtered product of  $u_i$  and Eq. (A.1) to obtain:

$$\begin{aligned} & \underbrace{\overline{u_i \frac{\partial u_i}{\partial t}} - \bar{u}_i \frac{\partial \bar{u}_i}{\partial t}}_{\text{Term 1}} + \underbrace{\overline{u_i \frac{\partial}{\partial x_j} (u_i u_j)} - \bar{u}_i \frac{\partial}{\partial x_j} (\bar{u}_i \bar{u}_j)}_{\text{Term 2}} \\ &= -\underbrace{\frac{1}{\rho} \left( \overline{u_i \frac{\partial p}{\partial x_i}} - \bar{u}_i \frac{\partial \bar{p}}{\partial x_i} \right)}_{\text{Term 3}} + \underbrace{\overline{\nu u_i \frac{\partial^2 u_i}{\partial x_j \partial x_j}} - \nu \bar{u}_i \frac{\partial^2 \bar{u}_i}{\partial x_j \partial x_j}}_{\text{Term 4}} + \underbrace{\bar{u}_i \frac{\partial \tau_{ij}^M}{\partial x_j}}_{\text{Term 5}}. \end{aligned} \quad (\text{A.7})$$

**A.1. Term 1**

We define the SGS kinetic energy as

$$k_{\text{sgs}} = \frac{1}{2} \tau_{ii}^{EV} \quad (\text{A.8})$$

and obtain

$$\begin{aligned} \overline{u_i \frac{\partial u_i}{\partial t}} - \bar{u}_i \frac{\partial \bar{u}_i}{\partial t} &= \frac{\partial}{\partial t} \left\{ \frac{1}{2} (\overline{u_i u_i} - \bar{u}_i \bar{u}_i) \right\} \\ &= \frac{\partial}{\partial t} \left\{ \frac{1}{2} (\tau_{ii}^{SS} + \tau_{ii}^{EV}) \right\} = \{\text{Eq. (A.8)}\} \\ &= \frac{\partial}{\partial t} \left( \frac{1}{2} \tau_{ii}^{SS} \right) + \frac{\partial k_{\text{sgs}}}{\partial t}. \end{aligned} \quad (\text{A.9})$$

**A.2. Term 2**

Assuming that the resolved and the total kinetic energy are

$$\bar{k} \equiv \frac{1}{2} \bar{u}_i \bar{u}_i, \quad k \equiv \frac{1}{2} \overline{u_i u_i}, \quad (\text{A.10})$$

we can model the total kinetic energy as

$$k = \bar{k} + k_{\text{sgs}} + \frac{1}{2} \tau_{ii}^{SS}, \quad (\text{A.11})$$

$$\begin{aligned} & \overline{u_i \frac{\partial}{\partial x_j} (u_i u_j)} - \bar{u}_i \frac{\partial}{\partial x_j} (\bar{u}_i \bar{u}_j) \\ &= \frac{1}{2} \frac{\partial}{\partial x_j} \left\{ \overline{u_i u_i u_j} - \bar{u}_i \bar{u}_i \bar{u}_j \right\} = \frac{\partial}{\partial x_j} \left\{ \frac{1}{2} \overline{u_i u_i u_j} - \bar{k} \bar{u}_j \right\} \\ &= \frac{\partial}{\partial x_j} \left\{ \frac{1}{2} \overline{u_i u_i u_j} - (k - k_{\text{sgs}} - \frac{1}{2} \tau_{ii}^{SS}) \bar{u}_j \right\}. \end{aligned} \quad (\text{A.12})$$

**A.3. Term 3**

$$-\frac{1}{\rho} \left( \overline{u_i \frac{\partial p}{\partial x_i}} - \bar{u}_i \frac{\partial \bar{p}}{\partial x_i} \right) = -\frac{1}{\rho} \frac{\partial}{\partial x_i} (\bar{u}_i \bar{p} - \bar{u}_i \bar{p}). \quad (\text{A.13})$$

**A.4. Term 4**

$$\begin{aligned} & \overline{\nu u_i \frac{\partial^2 u_i}{\partial x_j \partial x_j}} - \nu \bar{u}_i \frac{\partial^2 \bar{u}_i}{\partial x_j \partial x_j} \\ &= \nu \left\{ \frac{\partial}{\partial x_j} \left( \overline{u_i \frac{\partial u_i}{\partial x_j}} \right) - \frac{\partial u_i}{\partial x_j} \frac{\partial u_i}{\partial x_j} - \left[ \frac{\partial}{\partial x_j} \left( \bar{u}_i \frac{\partial \bar{u}_i}{\partial x_j} \right) - \frac{\partial \bar{u}_i}{\partial x_j} \frac{\partial \bar{u}_i}{\partial x_j} \right] \right\} \\ &= \nu \left\{ \frac{1}{2} \frac{\partial^2}{\partial x_j \partial x_j} (u_i u_i) - \frac{\partial u_i}{\partial x_j} \frac{\partial u_i}{\partial x_j} - \left[ \frac{1}{2} \frac{\partial^2}{\partial x_j \partial x_j} (\bar{u}_i \bar{u}_i) - \frac{\partial \bar{u}_i}{\partial x_j} \frac{\partial \bar{u}_i}{\partial x_j} \right] \right\} \\ &= \nu \left\{ \frac{\partial^2 k_{\text{sgs}}}{\partial x_j \partial x_j} + \frac{\partial^2}{\partial x_j \partial x_j} \left( \frac{1}{2} \tau_{ii}^{SS} \right) - \left( \frac{\partial u_i}{\partial x_j} \frac{\partial u_i}{\partial x_j} - \frac{\partial \bar{u}_i}{\partial x_j} \frac{\partial \bar{u}_i}{\partial x_j} \right) \right\}. \end{aligned} \quad (\text{A.14})$$

**A.5. Term 5**

$$\bar{u}_i \frac{\partial \tau_{ij}^M}{\partial x_j} = \frac{\partial}{\partial x_j} (\bar{u}_i \tau_{ij}^M) - \tau_{ij}^M \frac{\partial \bar{u}_i}{\partial x_j}. \quad (\text{A.15})$$

Substitution of Eqs. (A.9), (A.12)–(A.15) into Eq. (A.7) gives

$$\begin{aligned} & \frac{\partial k_{\text{sgs}}}{\partial t} + \frac{\partial}{\partial x_j} (\bar{u}_j k_{\text{sgs}}) \\ &= -\tau_{ij}^M \frac{\partial \bar{u}_i}{\partial x_j} - \frac{\partial}{\partial x_j} \left\{ \frac{1}{2} \overline{u_i u_i u_j} - k \bar{u}_j + \frac{1}{\rho} \bar{u}_j \bar{p} - \frac{1}{\rho} \bar{u}_j \bar{p} - \bar{u}_i \tau_{ij}^M \right\} \\ &+ \nu \frac{\partial^2 k_{\text{sgs}}}{\partial x_j \partial x_j} - \nu \left( \frac{\partial u_i}{\partial x_j} \frac{\partial u_i}{\partial x_j} - \frac{\partial \bar{u}_i}{\partial x_j} \frac{\partial \bar{u}_i}{\partial x_j} \right) \\ &+ \left\{ \nu \frac{\partial^2}{\partial x_j \partial x_j} \left( \frac{1}{2} \tau_{ii}^{SS} \right) - \frac{\partial}{\partial t} \left( \frac{1}{2} \tau_{ii}^{SS} \right) \right\} - \frac{\partial}{\partial x_j} \left\{ \frac{1}{2} \tau_{ii}^{SS} \bar{u}_j \right\}. \end{aligned} \quad (\text{A.16})$$

Now we model the SGS diffusion terms in Eq. (A.16)

$$D = -\frac{\partial}{\partial x_j} \left\{ \frac{1}{2} \overline{u_i u_i u_j} - k \bar{u}_j + \frac{1}{\rho} \bar{u}_j \bar{p} - \frac{1}{\rho} \bar{u}_j \bar{p} - \bar{u}_i \tau_{ij}^M \right\}$$

as

$$D = \frac{\partial}{\partial x_j} \left\{ v_{\text{sgs}} \frac{\partial k_{\text{sgs}}}{\partial x_j} \right\}. \quad (\text{A.17})$$

Although the diffusion term,

$$\frac{\partial}{\partial x_j} \left\{ \bar{u}_i \tau_{ij}^M \right\}, \quad (\text{A.18})$$

is computable, it is included in the model

$$D = \frac{\partial}{\partial x_j} \left\{ v_{\text{sgs}} \frac{\partial k_{\text{sgs}}}{\partial x_j} \right\} \quad (\text{A.19})$$

since it is not Galilean invariant.

The dissipation in Eq. (A.16)

$$\varepsilon_{k_{\text{sgs}}} = v \left( \frac{\partial \bar{u}_i}{\partial x_j} \frac{\partial \bar{u}_i}{\partial x_j} - \frac{\partial \bar{u}_i}{\partial x_j} \frac{\partial \bar{u}_i}{\partial x_j} \right) \quad (\text{A.20})$$

can be modeled as

$$\varepsilon_{k_{\text{sgs}}} = C_\varepsilon \frac{k_{\text{sgs}}^{3/2}}{\Delta}. \quad (\text{A.21})$$

We model the production term in Eq. (A.16), i.e. the SGS dissipation of the resolved kinetic energy,

$$\Pi = -\tau_{ij}^M \frac{\partial \bar{u}_i}{\partial x_j}, \quad (\text{A.22})$$

as

$$\Pi = \Pi^{\text{SS}} + \Pi_{k_{\text{sgs}}} = -\tau_{ij}^{\text{SS}} \frac{\partial \bar{u}_i}{\partial x_j} - \tau_{ij}^{\text{EV}} \frac{\partial \bar{u}_i}{\partial x_j}. \quad (\text{A.23})$$

From this, we obtain the modeled  $k_{\text{sgs}}$  equation for the mixed one-equation model:

$$\begin{aligned} \frac{\partial k_{\text{sgs}}}{\partial t} + \frac{\partial}{\partial x_j} \left( \bar{u}_j k_{\text{sgs}} \right) \\ = \Pi_{k_{\text{sgs}}} + \frac{\partial}{\partial x_j} \left\{ (v_{\text{sgs}} + v) \frac{\partial k_{\text{sgs}}}{\partial x_j} \right\} - C_\varepsilon \frac{k_{\text{sgs}}^{3/2}}{\Delta} \\ + \Pi^{\text{SS}} + v \frac{\partial^2}{\partial x_j \partial x_j} \left( \frac{1}{2} \tau_{ii}^{\text{SS}} \right) - \frac{\partial}{\partial t} \left( \frac{1}{2} \tau_{ii}^{\text{SS}} \right) - \frac{\partial}{\partial x_j} \left\{ \frac{1}{2} \tau_{ii}^{\text{SS}} \bar{u}_j \right\}. \end{aligned} \quad (\text{A.24})$$

## References

- Bardina, J., Ferziger, J., Reynolds, W., 1980. Improved subgrid scale models for large eddy simulation. AIAA paper 80-1357, Snowmass, Colorado.
- Carati, D., Ghosal, S., Moin, P., 1995. On the representation of backscatter in dynamic localization models. *Phys. Fluids* 7, 606–616.
- Comte-Bellot, G., Corrsin, S., 1971. Simple Eulerian time correlation of full- and narrow-band velocity signals in grid-generated, ‘isotropic’ turbulence. *J. Fluid Mech.* 48, 273–337.
- Davidson, L., 1997. Large eddy simulation: a dynamic one-equation subgrid model for three-dimensional recirculating flow. In: 11th

- International Symposium on Turbulent Shear Flow, Grenoble, vol. 3, pp. 26.1–26.6.
- Davidson, L., 2001. Hybrid LES-RANS: a combination of a one-equation SGS model and a  $k-\omega$  model for predicting recirculating flows. In: ECCOMAS CFD Conference, Swansea, UK.
- Domaradzki, J.A., Liu, W., Brachet, M.E., 1993. An analysis of subgrid-scale interactions in numerically simulated isotropic turbulence. *Phys. Fluids* 5, 1747–1759.
- Domaradzki, J.A., Liu, W., Härtel, C., Kleiser, L., 1994. Energy transfer in numerically simulated wall-bounded turbulent flows. *Phys. Fluids* 6, 1583–1599.
- Emin, P., 1997. The full multigrid method applied to turbulent flow in ventilated enclosures using structured and unstructured grids. Ph.D. Thesis, Department of Thermo and Fluid Dynamics, Chalmers University of Technology, Gothenburg.
- Fureby, C., Tabor, G., 1997. Mathematical and physical constraint on large-eddy simulations. *Theoret. Comput. Fluid Dyn.* 9, 85–102.
- Germano, M., 1986. A proposal for a redefinition of the turbulent stresses in the filtered Navier–Stokes equations. *Phys. Fluids* 7, 2323–2324.
- Ghosal, S., 1999. Mathematical and physical constraint on large-eddy simulations of turbulence. *AIAA J.* 37, 425–433.
- Ghosal, S., Lund, T., Moin, P., Akselvoll, K., 1995. A dynamic localization model for large-eddy simulation of turbulent flows. *J. Fluid Mech.* 286, 229–255.
- Ghosal, S., Moin, P., 1995. The basic equations for the large eddy simulation of turbulent flows in complex geometry. *J. Comput. Phys.* 118, 24–37.
- Kim, J., Moin, P., Moser, R., 1987. Turbulence statistics in fully developed channel flow at low Reynolds number. *J. Fluid Mech.* 177, 133–166.
- Krajnović, S., Davidson, L., 1999. Large-eddy simulation of the flow around a surface-mounted cube using a dynamic one-equation subgrid model. In: Banerjee, S., Eaton, J. (Eds.), *The First International Symposium on Turbulence and Shear Flow Phenomena*. Begell House Inc., New York, Wallingford, UK, pp. 741–746.
- Krajnović, S., Davidson, L., 2001. Large eddy simulation of the flow around a three-dimensional bluff body. In: 39th AIAA Aerospace Sciences Meeting and Exhibit, AIAA paper 2001-0432, Reno, Nevada, USA.
- Lilly, D., 1992. A proposed modification of the Germano subgrid-scale closure method. *Phys. Fluids* 4, 633–635.
- Liu, S., Meneveau, C., Katz, J., 1994. On the properties of similarity subgrid-scale models as deduced from measurements in a turbulent jet. *J. Fluid Mech.* 275, 83–119.
- Martinuzzi, R., Tropea, C., 1993. The flow around surface-mounted prismatic obstacles placed in a fully developed channel flow. *ASME: J. Fluids Eng.* 115, 85–91.
- Meneveau, C., Katz, J., 2000. Scale-invariance and turbulence models for large-eddy simulation. *Ann. Rev. Fluid Mech.* 32, 1–32.
- Menon, S., Kim, W.-W., 1996. High Reynolds number flow simulations using the localized dynamic subgrid-scale model. In: 34th Aerospace Sciences Meeting, AIAA paper 96-0425, Reno.
- Piomelli, U., Moin, P., Ferziger, J.H., 1988. Model consistency in large eddy simulation of turbulent channel flows. *Phys. Fluids* 7, 1884–1891.
- Rhie, C., Chow, W., 1983. Numerical study of the turbulent flow past an airfoil with trailing edge separation. *AIAA J.* 21, 1525–1532.
- Ribault, C.L., Sarkar, S., Stanley, S.A., 1999. Large eddy simulation of a plane jet. *Phys. Fluids* 11, 3069–3083.
- Rodi, W., 1976. A new algebraic relation for calculating the Reynolds stresses. *ZAMM* 56, T219–T221.
- Sarghini, F., Piomelli, U., 1999. Scale-similar models for large-eddy simulations. *Phys. Fluids* 11, 1596–1607.

- Sohankar, A., Davidson, L., Norberg, C., 2000a. Large eddy simulation of flow past a square cylinder: comparison of different subgrid scale models. *ASME: J. Fluids Eng.* 122 (1), 39–47.
- Sohankar, A., Davidson, L., Norberg, C., 2000b. Erratum. *ASME: J. Fluids Eng.* 122 (3), 643.
- Speziale, C., 1985. Galilean invariance of subgrid-scale stress models in the large-eddy simulation of turbulence. *J. Fluid Mech.* 156, 55–62.
- Vreman, B., Geurts, B., Kuerten, H., 1994a. On the formulation of the dynamic mixed subgrid-scale model. *Phys. Fluids* 6, 4057–4059.
- Vreman, B., Geurts, B., Kuerten, H., 1994b. Realizability conditions for the turbulent stress tensor in large-eddy simulation. *J. Fluid Mech.* 278, 351–362.
- Zang, Y., Street, R., Koseff, J., 1993. A dynamic mixed subgrid-scale model and its application to turbulent recirculating flows. *Phys. Fluids* 5, 3186–3196.